Applied Catalysis B: Environmental 198 (2016) 398–403

Contents lists available at ScienceDirect

Applied Catalysis B: Environmental

journal homepage: www.elsevier.com/locate/apcatb

Facile surface treatment on Cu_2O photocathodes for enhancing the photoelectrochemical response

Dawei Cao[a,1], Nasori Nasori[a,1], Zhijie Wang[a,b], Liaoyong Wen[a], Rui Xu[a], Yan Mi[a], Yong Lei[a,*]

[a] Institute of Physics & IMN MacroNano(ZIK), Ilmenau University of Technology, 98693 Ilmenau, Germany
[b] Key Laboratory of Semiconductor Materials Science, Beijing Key Laboratory of Low Dimensional Semiconductor Materials and Devices, Institute of Semiconductors, Chinese Academy of Sciences, Beijing 100083, China

ARTICLE INFO

Article history:
Received 4 January 2016
Received in revised form 27 May 2016
Accepted 2 June 2016
Available online 3 June 2016

Keywords:
P-type Cu_2O
Surface treatment
Photoelectrochemistry
Photocathode

ABSTRACT

P-type Cu_2O has long been regarded as an advantageous material in photoelectrochemistry, owing to the suitable band gap structure and cost-effective production. However, such promising material is suffering from corrosion in aqueous electrolytes. To address this issue and attain a high photoelectrochemical performance, protective oxide layers and expensive catalysts have to be adopted. The complicacy of such additional procedures, however, limits the further applications. Instead of utilizing surface protecting oxide layers and expensive catalysts, herein, we report that the surface treatment of Cu_2O photocathodes using trisodium citrate (TSC) could also greatly enhance the photoelectrochemical performance. In comparison with the electrode without TSC, the photocathode of FTO/Au/Cu_2O/TSC/TiO_2/Pt presents a pronounced increment in photocurrent with a factor of about 2. Therefore, this paper provides a novel but convenient methodology to optimize the performance of solar energy conversion systems employing p-type Cu_2O by modifying the surface with functional molecules.

1. Introduction

Harvesting solar energy and storing it in chemical bonds, particularly in the simplest chemical bond like H_2, could be a highly feasible approach to solving the world-wide energy challenge. Although p-type Cu_2O has long been considered as an attractive candidate for water splitting due to the favourable band gap position and high abundance of elements [1–3], concomitant surface defects like reconstructions, uncoordinated atoms and even the CuO or Cu phases generated in the synthesizing or measuring procedures, adversely impact the device efficiency and stability [4,5]. Specifically, the presence of Cu(II) or Cu(0) sites on the surface severely deteriorates the device performance and it is highly required to prepare Cu_2O photocathode with high crystal quality and to avoid the formation of such surface impurities [6,7]. An advantageous approach for electrodepositing Cu_2O is depositing the material on FTO/Au substrates rather than on FTO or FTO/Cu substrates. The existence of Au thin film helps to improve the crystal quality and performance reproducibility for the grown Cu_2O film [2,8]. Even in this case, the electronic properties of the resulting material could not be optimized for the photoelectrochemical (PEC) performance.

Though the utilization of thin oxide layers can protect Cu_2O from corrosion during measurements [2,5], it is still difficult to change electronic properties of Cu_2O just using the post-solid-state treatment. Herein, we report an effective surface treatment method for attaining a high PEC performance on Cu_2O based photocathodes. The surface treatment was conducted by soaking the as-grown films in a trisodium citrate (TSC) aqueous solution and the subsequent electrochemical characterizations illustrated that the doping level of the Cu_2O films was impressively enhanced along with an enlarged band bending at the interface of Cu_2O/electrolyte. Accordingly, the photocurrent of the corresponding PEC electrodes with the subsequent protection layer (TiO_2/Pt) was ameliorated around two times. Aspects relevant to the charge transfer dynamics were particularly investigated by transient photoluminescence spectroscopy.

* Corresponding author at: Ilmenau University of Technology, Heliosbau 1102, Prof. Schmidt-Straße 26, Germany.
E-mail address: yong.lei@tu-ilmenau.de (Y. Lei).
[1] These authors contributed equally to this work.

http://dx.doi.org/10.1016/j.apcatb.2016.06.010
0926-3373/

2. Experimental

2.1. Preparation of the Cu_2O films

First, FTO glass was cleaned with acetone, ethanol and DI water, respectively. Then, a thin layer of Au (25 nm) was deposited on the cleaned and dried FTO glass as the substrate via a physical vapour deposition procedure. Subsequently, Cu_2O thin films were cathodically electrodeposited from a 0.4 M copper sulphate bath containing 3 M lactic acid. The pH value of the bath was carefully adjusted to 12.0 by the addition of 3 M sodium hydroxide. Films were grown at a constant potential of −0.40 V vs Ag/AgCl in a normal three-electrode configuration for a nominal duration of 30 min. The temperature of the bath was controlled at 45 °C using a heating plate with an in situ temperature probe. For comparison, we also prepared Cu_2O thin films on FTO glass directly using the same procedure. Finally, the prepared Cu_2O films were purposely soaked in an aqueous solution containing 1 M TSC for 30 min and dried by N_2.

2.2. Deposition of TiO_2 and Pt nanoparticles

The samples were put in an atomic layer deposition (ALD, Picosun Sunale R150) chamber for depositing the protection layer of TiO_2 and Pt catalyst. Titanium dioxide was deposited using titanium (IV) chloride ($TiCl_4$), and distilled-water (H_2O) as the Ti and O precursors, respectively. The TiO_2 deposition was then carried out at 200 °C and one typical cycle consists of: $TiCl_4$-N_2 purge-H_2O-N_2 purge (1 cycle). The growth rate of TiO_2 is about 0.6 nm per cycle. Deposition of Pt nanoparticles was performed on the reactor with low-nitrogen-filling ALD process as we previously reported [9]. The precursors used for Pt growth were trimethyl (methyl cyclopentadienyl) platinum (IV) (Pt(MeCp)Me_3) and O_2. The temperature of Pt precursor was held at 80 °C. The substrate temperature was controlled at 220 °C. And the typical ALD cycle consisted of Pt(MeCp)Me_3 pulsing (1.0 s)-low N_2 filling (60 s)-N_2 purging (30 s)-O_2 pulsing (1.0 s)-low N_2 filling (30 s)-N_2 purging (30 s).

2.3. Fabrication of Cu_2O photocathodes

A strip of conductive copper tape was stuck on the exposed FTO part of the specimens to extend the conducting circuit and threaded through a glass tube and then sealed with an insulating epoxy. Electrode areas were optically measured as 0.2 cm^2.

2.4. Photoelectrochemical measurements

External quantum yield (EQY) was measured with an Oriel 150 W Xe arc lamp (Newport) and a quarter-turn single-grating monochromator (Newport). Sample measurements were recorded with chopped illumination. The output current signal was connected to a Merlin digital lock-in radiometry system and the output signal from the lock–in amplifier was fed into a computer controlled by TRACQ BASIC software. Current–potential plots and impedance characterization were measured using the digital BioLogic potentiostat (SP-200) and 0.1 M sodium sulphate aqueous solution served as the electrolyte. A Pt counter electrode and Ag/AgCl reference electrode were used during the measurements. A standard 300 W Xe lamp (Newport) served as the light source and the light intensity was characterized to 100 mW cm^{-2} by a Si photodiode (Newport).

2.5. Characterizations

The X-ray diffraction (XRD) pattern was recorded on Bruker D8 Advance equipped with graphite monochromatized high-intensity Cu Kα radiation (λ = 1.54178 Å). The scanning electron microscopy (SEM) images were obtained by S4800 HITACHI (Japan) scanning electron microscope. Room–temperature UV–vis absorption spectroscopy was measured using Varian Cary 5000 UV–vis-NIR spectrophotometer. X-ray photoelectron spectroscopy (XPS) experiments were carried out on an Axis Ultra DLD system (Shimadzu) using Al Kα radiation (hv = 1486.6 eV). The whole spectra (0–1200 eV) and the narrow spectra of all the elements with high resolution were both recorded by using the RBD 147 interface (RBD Enterprises, USA) through the Auger Scan 3.21 software. Binding energies were calibrated by using the containment carbon (C1s = 284.6 eV). Fourier transform infrared (FTIR) spectra were recorded at room temperature using FTS-60 V FTIR spectrophotometer. In transient photoluminescence measurements, the specimens were optically excited by a 420 nm SHG (second harmonic generation) signal from a femtosecond Ti: sapphire laser system, with a repetition rate of 80 MHz. The photoluminescence signal from the sample was collected by a NA = 0.42 lens and sent to a 0.75 m focal length spectrometer. Time-integrated photoluminescence was detected by a liquid-nitrogen cooled Si-CCD, while the photoluminescence lifetime was analysed by an avalanche photodiode together with a time-correlated single-photon counting module.

3. Results and discussion

The electrodeposition for Cu_2O was performed in a copper sulphate bath containing 3 M lactic acid. The bath pH value was carefully adjusted to 12.0 by precisely controlled addition of 3 M NaOH. Herein, the use of pH buffers was intentionally avoided to preclude interferences from the buffer components with the interfacial behaviour. The deposition potential was set as −0.40 V vs Ag/AgCl according to the cyclic voltammetry test shown in Supporting information Fig. S1, where the reduction peak of Cu^{2+} to Cu^{+} at −0.40 V vs Ag/AgCl could be clearly observed. Fig. 1a portrays the representative SEM images of the prepared films on FTO/Au substrates. The films are constructed by continuously distributed polyhedral particles. The size of these particles is gauged as 1−3 μm. For the films grown on FTO glass, however, the size of the composed particles becomes bigger and the configuration turns out to be cuboid, as demonstrated in Fig. 1b. Though it is well reported that the morphology of Cu_2O nanoparticles can be determined by the pH values, surface ligands and profiles of the growing seeds [10,11], these data point out that the morphology could also be influenced by the choice of depositing substrates, which contributes another factor to manipulate the morphology of the Cu_2O nanoparticles. XRD pattern of the Cu_2O films is given in Fig. 1c, where the diffraction peaks at 29.6°, 36.5°, 42.4°, 61.4° and 73.6° can be doubtlessly ascribed to the diffraction of (110), (111), (200), (220) and (311) planes of Cu_2O (JCPDS card No. 05-0667) [4]. The crystalline structure is depicted as the inset of Fig. 1c. Diffraction peaks of CuO and Cu are not discernible, implying a pure Cu_2O structure in the films. In addition, consistent with the reported values [12–14], the band gap of the synthesized Cu_2O is characterized as 2.09 eV by the absorption analyses shown in Fig. 1d and inset I. Such suitable value qualifies the resultant as a good material in solar energy conversion. The absorption spectrum of Au thin film that exhibits a slight absorption capability in the range of 400–800 nm is also presented. To investigate the absorption capability of the photocathodes furthermore, finite difference time domain (FDTD) simulation was performed for the structure, FTO/Au/Cu_2O. Inset II in Fig. 1d shows the relevant spatial distribution of the electric field intensity across the structure illuminated by the photons at 500 nm and the polyhedral feature of the particles in the film strengthens the absorption efficiency by the scattering effect. Supporting information Fig. S2 shows the calculated absorption efficiency in

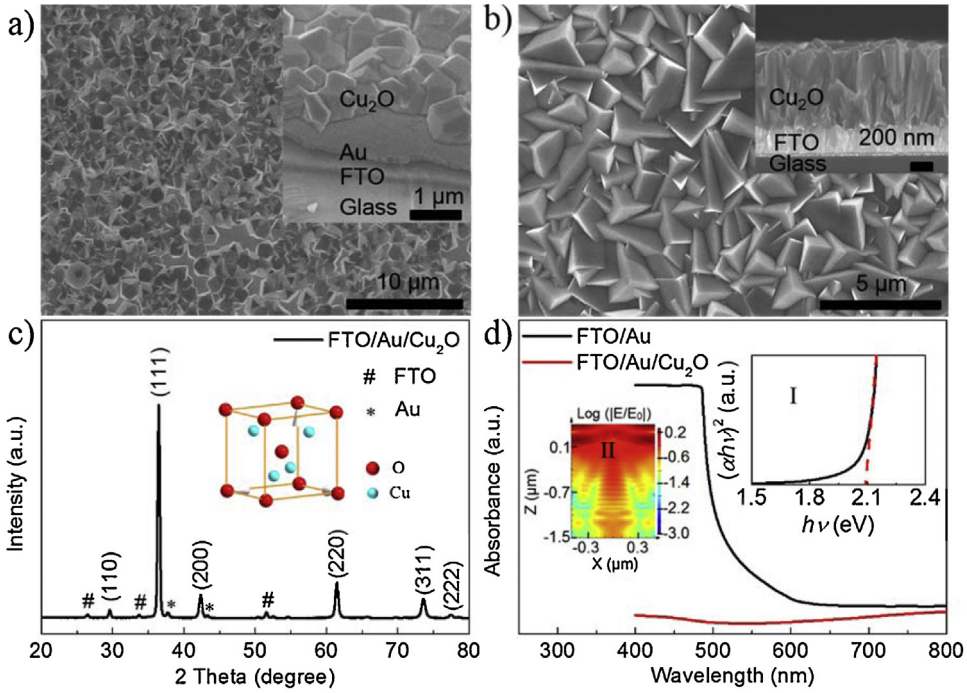

Fig. 1. (a,b) SEM images of the prepared Cu_2O films on FTO/Au and FTO substrates, the insets show the cross-sectional SEM images. (c) XRD pattern of the Cu_2O films on FTO/Au substrates. The inset presents the crystal structure of the material. (d) Absorption spectroscopic measurements of the samples. Inset I: plot of $(\alpha h\nu)^2$ vs $h\nu$ for estimating the band gap value of the film. Inset II: spatial distribution of the electric field intensity across the photocathodes illuminated by the photons at 500 nm.

accordance with the thickness of Cu_2O on FTO/Au. As we tune the thickness from 500 nm to 2000 nm, the absorption efficiencies show a close value below 500 nm, due to the high absorption coefficient of Cu_2O. In the longer wavelength region, the thickness begins to impact the absorption by increasing the intensity and the interference effect attributing to the surface nanostructure could also be influential.

Though XRD pattern of the prepared Cu_2O films presents a pure Cu_2O phase, it is still hard to exclude the existence of Cu (II) and Cu (0) impurities on the surface. To characterize it more convincingly, X-ray photoelectron spectroscopy (XPS) was specifically studied. As shown in Fig. 2a, the Cu 2p peaks are resolved and the main peaks at 932.5 and 952.6 eV correspond to the Cu $2p_{3/2}$ and Cu $2p_{1/2}$, respectively, assigning to the Cu^+ [4,15]. In the Cu 2p spectrum, Cu^{2+} is identified by the emergence of a main signal at 933.6 eV along with a series of shakeup satellites between 932.5 and 952.6 eV [16]. For the sample without any surface treatments, the satellite peaks are quite prominent and only slightly lower than the Cu $2p_{1/2}$ peak, indicative of the presence of Cu^{2+} on the surface. These shakeup satellite peaks are characteristic of Cu^{2+} that has a partially filled Cu $3d^9$ shell configuration in the ground state [4,17], which usually deteriorates p-type feature of Cu_2O.

To fix the Cu^{2+} related impurities on the prepared Cu_2O films and to stabilize the photocathodes, a post-solid-state surface treatment

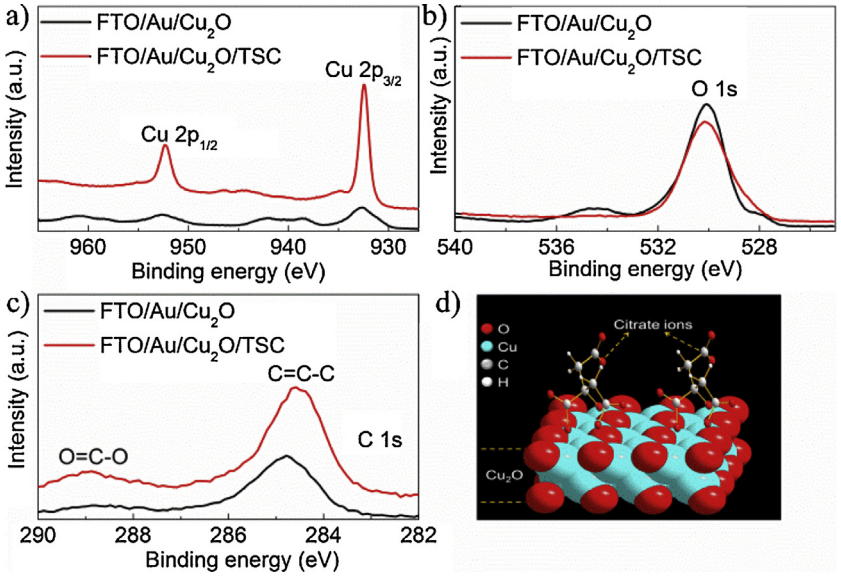

Fig. 2. (a–c) XPS spectra of the as-prepared Cu_2O thin films with different surface conditions. The spectra display the resolved peaks of Cu 2p, O 1s and C 1s, respectively. (d) Schematic of the TSC modified Cu_2O surface.

was carried out by soaking the Cu_2O films in a 1 M TSC aqueous solution for 30 min. TSC that is well known as the chelating agent in the synthesis of Cu_2O nanoparticles could help to avoid the formation of $Cu(OH)_2$ and CuO in the reducing reactions of Cu^{2+} [11,18]. In addition, the reducing capability of TSC could also probably influence the Cu $3d^9$ shell configuration by making it more filled. As displayed in Fig. 2a, after surface treatment, the two main peaks become much more outstanding as compared with the peaks from the same films without surface treatment. To be highlighted, the satellite peaks turn out to be ignorable, indicative of the feasibility for this peculiar treatment. The absence of sharp satellite features for Cu_2O is rationalized on the basis of a full Cu $3d^{10}$ shell that inhibits screening via charge transfer involving d states [4]. Fig. 2b exhibits the O 1s spectra of the sample before and after the surface treating procedure. The main peak signal at 530.5 eV is a clear oxygen signature associated with Cu_2O [4] and the treatment in TSC solution is beneficial for eliminating the impurity peaks around O 1s main peak, yielding an efficient platform for charge transfer. Regarding the C 1s spectra given in Fig. 2c, the peaks for C═C—C and O═C—O [19] are both amplified by soaking the Cu_2O films in the solution, demonstrative of that the TSC molecules are linked on the Cu_2O surface and could protect the films from deterioration in the subsequent measuring procedures. To describe this statement straightforwardly, we present the schematic for the TSC modified Cu_2O surface, as shown in Fig. 2d. FTIR spectra further verify the adsorption of TSC on the surface of Cu_2O, as shown in Supporting information Fig. S3. Compared to the naked FTO/Au/Cu_2O sample, FTIR spectrum of the FTO/Au/Cu_2O/TSC exhibits the characteristic absorption peaks of carboxyl group of sodium citrate, such as 1600 cm^{-1} and 1392 cm^{-1} due to the —COO— symmetric and antisymmetric stretching respectively [20].

Electronically, such surface modification could also positively impact the doping levels of the Cu_2O films and band bending of the photocathodes when contacted with the electrolyte. Electrochemical impedance investigations were performed by soaking the FTO/Au/Cu_2O electrode in a 0.1 M Na_2SO_4 aqueous solution as the working electrode. A Pt counter electrode and Ag/AgCl reference electrode were used during the measurements. Fig. 3a shows Mott-Schottky plots at a fixed frequency of 1 kHz for the electrodes with different surface conditions, where a typical p-type feature could be obviously observed. Noteworthily, these plots yield apparent flat band potentials of 0.20 V and 0.15 V vs Ag/AgCl for the same photocathode before and after experiencing the surface treatment, respectively. The treatment shifts the flat band potentials negatively and thus results in a strengthened band bending at Cu_2O/electrolyte interface that is profitable for transferring the photo-generated electrons to the surface. Using slopes of the plots, doping densities were calculated as 1.06×10^{19} cm^{-3} and 1.53×10^{19} cm^{-3}, respectively. The details of the relative calculation can be found in Supporting information. The surface treatment enhances the doping levels and thus the resistance of the system can be accordingly reduced. As exhibited in the inset of Fig. 3a, the Nyquist plots covering the frequency of 10^5–1 Hz at the bias of −0.6 V vs Ag/AgCl demonstrates that charge transfer resistance of the system is prominently decreased by the usage of TSC, given that the semicircle in a Nyquist plot at high frequencies is characteristic of the charge transfer process and the diameter of the semicircle is estimated to be equal to the charge transfer resistance [21,22]. This series of electrochemical measurements illustrates that modification of Cu_2O with TSC is able to positively impact the electronic properties of Cu_2O, by increasing the doping density and enlarging the band bending at the interface with electrolyte. These are beneficial for promoting the separation and transfer of the photo-generated charge carriers.

Moreover, ascribing to the reduction of Cu (II) impurities, the transfer of photo-generated charges could be facilitated, since impurities have a negative effect on charge transfer and transport. Fig. 3b shows two representative time-resolved photoluminescence decays after pulsed excitation at λ = 420 nm. Obviously, both of the curves present a rapid decay feature in nanosecond scale, which is in agreement with the reports [23,24]. To be noteworthy, the samples that experienced surface treatment yield a faster decay time as compared with the intrinsic samples, indicating an accelerated charge transfer mechanism induced by the modification of TSC. Using the conventional single exponential model to fit the curves, lifetimes of 0.59 ns and 0.48 ns for the same sample before and after surface treatment were acquired. Table S1 in Supporting information provides all the fitting parameters. The accelerated charge transfer is bound to enhance the possibility for photo-generated charges contributing to the photocurrent, instead of making them recombine radiatively. The steady state photoluminescence spectra are shown in the inset of Fig. 3b. The peak located at around 570 nm is associated with the near band emission [25,26]. By comparing the two spectra, the photoluminescence intensity of the Cu_2O film is markedly reduced to its 30% after the surface treatment, which illustrates that the radiative recombination of the photo-generated charges is efficaciously inhibited. The normalized PL spectra are given in Supporting information Fig. S4, which shows that these two peaks have a close broadness. The result indicates that the treatment with TSC could only quench the PL intensity and the intrinsic optical property is nearly uninfluential.

The above analyses point out a great potential to apply this surface treatment for improving the PEC response of Cu_2O based photocathodes. First, by following the conventional photocathode structure for Cu_2O, we fabricated the FTO/Au/Cu_2O/TSC/TiO_2/Pt electrodes. The according SEM image and XRD pattern for FTO/Au/Cu_2O/TSC/TiO_2 are given in Supporting information Fig. S5 and these data evidence the presence of compact TiO_2 layer on Cu_2O, which can protect the layer from electrochemical deterioration. The Pt layer behaves as the catalyst for hydrogen generation.

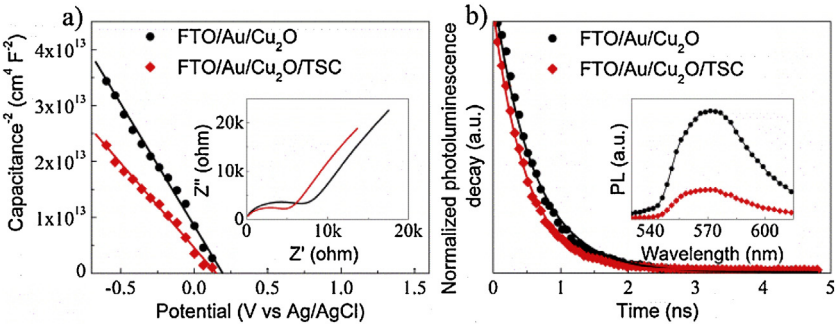

Fig. 3. (a) Mott-Schottky plots with Nyquist plots as the inset. (b) Time-resolved photoluminescence decay curves (excitation: 420 nm), the inset shows the steady state photoluminescence spectra (excitation: 420 nm).

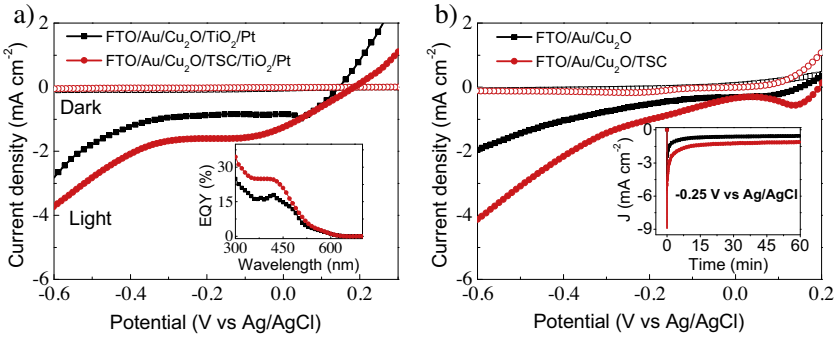

Fig. 4. (a) and (b) Current density-potential curves of the Cu_2O based photocathodes with different surface conditions. Inset of (a): EQY spectra of the FTO/Au/Cu_2O/TiO_2/Pt photoelectrode with and without TSC; Inset of (b): Curves of the time-dependent photocurrent measured for the FTO/Au/Cu_2O photoelectrode without/with TSC under AM1.5G (100 mW cm^2) illumination.

The current density–potential (J–V) characteristics of these electrodes under 100 mW cm^{-2} of solar simulated light are shown in Fig. 4a. All these J–V curves exhibit a cathodic photocurrent and indicate a distinct p-type feature of the prepared Cu_2O films, consistent with the Mott-Schottky measurements. To be exciting, the FTO/Au/Cu_2O/TSC/TiO_2/Pt electrode delivers an increase of around two times in photocurrent by comparing with the electrode without surface treatment. The photocurrent is realized as high as 3.8 mA cm^{-2} at −0.6 V vs Ag/AgCl. The EQY spectra shown as the inset of Fig. 4a present the same tendency with that in the J-V analysis. The profiles of these spectra are in agreement with the absorption spectrum of the material, supporting that the photocurrent is from the charges generated in Cu_2O. Curves of photocurrent vs time curve under interval on-off light irradiation of the FTO/Au/Cu_2O/TiO_2/Pt and FTO/Au/Cu_2O/TSC/TiO_2/Pt electrodes are given in Supporting information Fig. S6. The data demonstrate a fast photoelectrochemical response of the electrodes.

Meanwhile, we also checked the PEC performance of the electrodes without the passivation layer of TiO_2 and the relevant results are given in Fig. 4b. As we expect, the photocurrent of bare FTO/Au/Cu_2O electrodes could also be enhanced dramatically by the surface treatment. The according photocurrent is obtained as 4.2 mA cm^{-2} at −0.6 V vs Ag/AgCl, even better than that from the FTO/Au/Cu_2O/TSC/TiO_2/Pt electrode. To check the stability of the photocathodes, we measured the photocurrent at a fixed potential and the transient curves are shown in the inset. Though these curves present a decay feature at the initial period after light illumination, the photocurrents are quite stable after 30 s and can be maintained more than one hour. To be noted, photocurrent of the FTO/Au/Cu_2O photoelectrode treated by TSC is always higher than that from the corresponding bare sample. Such observation confirms that the benefit of TSC to improve the PEC performance of Cu_2O is sustainable and the presence of the molecule on the surface could also be possible to improve the device stability. For checking the stability of the Cu_2O surface after TSC modification even after PEC measurement, atomic force microscopic measurement (AFM) was performed. As shown in Supporting information Fig. S7, we cannot observe obvious changes of morphology. This indicates that increase of photocurrent is not from the change in surface area and the surface is stable even after PEC measurement. Raman spectra in Supporting information Fig. S8 can further prove this conclusion. To check the feasibility of such surface treatment to other Cu_2O involved systems, we also fabricated Cu_2O electrodes on FTO directly without the Au thin layer. As shown in Supporting information Fig. S9, the corresponding J–V curves and EQY spectra exhibit the same trend as that in FTO/Au/Cu_2O electrodes, though the performance is lower. As reported by Zhang et al. [27], the multi-facet Cu_2O nanoparticles have a superior photocatalytic property over the cubic counterparts and our observations support their points.

Collectively, we could reach a conclusion for benefits of Au layer to the improvement of PEC performance. First, the highly conductive nature has two contributions. One is good for realization of the highly crystalline Cu_2O film with photocatalytic active polyhedral morphology, and the other one is favourable for collecting the photo-generated electrons efficiently. Second, the surface plasmon effect of the Au layer contributes to the absorption of solar energy and the resulting excited energy could promote the PEC reactions by hot charge or energy transfer to Cu_2O and then to the electrolyte. Third, the scattering effect of Au layer is beneficial for enhancing the solar energy absorption by Cu_2O.

These data indicate that this peculiar surface modification procedure is able to fix the impurities on Cu_2O surface and thereby strengthen the p-type feature of the corresponding Cu_2O film. Accordingly, the PEC performance is dramatically improved via this convenient and cost-less treatment. Regarding that there is a large variety of molecules with multiple functions, our methodology provides a feasible means to optimize the solar energy conversion efficiency of the Cu_2O involved devices from the aspects of ameliorating the surface quality of Cu_2O, protecting the films from deterioration, extending the photon absorption range beyond the absorption threshold of Cu_2O, and even promoting the PEC energy conversion reactions by introducing catalytic effects [4,28,29].

4. Conclusion

Summarily, we have developed a simple surface treatment approach for the Cu_2O based photocathodes to enhance the PEC performance. The adopted TSC is beneficial for fixing the Cu (II) impurities, increasing the doping density of Cu_2O films and conducting the photo-generated charge carriers to the interface with electrolyte. Accordingly, a great improvement in photocurrent and EQY is achieved. Thus, this paper offers a cost-advantageous methodology to optimize the overall efficiency of solar energy conversion systems that utilize Cu_2O as light-harvesting component.

Acknowledgments

This work is financially supported by the European Research Council (ThreeDsurface, 240144), BMBF (ZIK-3DNanoDevice, 03Z1MN11), BMBF (Meta-ZIK-BioLithoMorphie, 03Z1M511), German Research Foundation (DFG: LE 2249_4-1), Hundred-Talent Program (Chinese Academy of Sciences), Beijing Natural Science Foundation (2162042) and National Natural Science Foundation of China (21503209). Dr. Dawei Cao sincerely thanks the support from the Alexander von Humboldt Foundation. Nasori Nasori thanks the support from the Bureau of Planning and International Cooperation of the Ministry of Education and Culture of the Republic Indonesia.

Appendix A. Supplementary data

Supplementary data associated with this article can be found, in the online version, at http://dx.doi.org/10.1016/j.apcatb.2016.06.010.

References

[1] M. Hara, T. Kondo, M. Komoda, S. Ikeda, J.N. Kondo, K. Domen, M. Hara, K. Shinohara, A. Tanaka, Chem. Commun. 2 (1998) 357.
[2] A. Paracchino, V. Laporte, K. Sivula, M. Grätzel, E. Thimsen, Nat. Mater. 10 (2011) 456.
[3] C. Xiang, G.M. Kimball, R.L. Grimm, B.S. Brunschwig, H.A. Atwater, N.S. Lewis, Energy Environ. Sci. 4 (2011) 1311.
[4] H. Azimi, S. Kuhri, A. Osvet, G. Matt, L.S. Khanzada, M. Lemmer, N.A. Luechinger, M.I. Larsson, E. Zeira, D.M. Guldi, C.J. Brabec, J. Am. Chem. Soc. 136 (2014) 7233.
[5] A. Paracchino, N. Mathews, T. Hisatomi, M. Stefik, S.D. Tilley, M. Grätzel, Energy Environ. Sci. 5 (2012) 8673.
[6] Z. Zheng, B. Huang, Z. Wang, M. Guo, X. Qin, X. Zhang, P. Wang, Y. Dai, J. Phys. Chem. C 113 (2009) 14448.
[7] L. Wu, L. Tsui, N. Swami, G. Zangari, J. Phys. Chem. C 114 (2010) 11551.
[8] Y.S. Lee, J. Heo, S.C. Siah, J.P. Mailoa, R.E. Brandt, S.B. Kim, R.G. Gordon, T. Buonassisi, Energy Environ. Sci. 6 (2013) 2112.
[9] Y. Mi, L. Wen, Z. Wang, D. Cao, H. Zhao, Y. Zhou, F. Grote, Y. Lei, Catal. Today 262 (2016) 141.
[10] Y. Xu, H. Wang, Y. Yu, L. Tian, W. Zhao, B. Zhang, J. Phys. Chem. C 115 (2011) 15288.
[11] M.D. Susman, Y. Feldman, A. Vaskevich, I. Rubinstein, ACS Nano 8 (2014) 162.
[12] S. Brittman, Y. Yoo, N.P. Dasgupta, S.I. Kim, B. Kim, P. Yang, Nano Lett. 14 (2014) 4665.
[13] Y. Nakano, S. Saeki, T. Morikawa, Appl. Phys. Lett. 94 (2009) 3.
[14] B.K. Meyer, A. Polity, D. Reppin, M. Becker, P. Hering, P.J. Klar, T. Sander, C. Reindl, J. Benz, M. Eickhoff, C. Heiliger, M. Heinemann, J. Bläsing, A. Krost, S. Shokovets, C. Müller, C. Ronning, Phys. Status Solidi B 249 (2012) 1487.
[15] R. Ji, W. Sun, Y. Chu, ChemPhysChem 14 (2013) 3971.
[16] S. Poulston, P.M. Parlett, P. Stone, M. Bowker, Surf. Interface Anal. 24 (1996) 811.
[17] Y.K. Hsu, C.H. Yu, Y.C. Chen, Y.G. Lin, Electrochim. Acta 105 (2013) 62.
[18] Y. Sui, W. Fu, Y. Zeng, H. Yang, Y. Zhang, H. Chen, Y. Li, M. Li, G. Zou, Angew. Chem. Int. Ed. 49 (2010) 4282.
[19] X. An, K. Li, J. Tang, ChemSusChem 7 (2014) 1086.
[20] C. Cheng, Y. Wen, X. Xu, H. Gu, J. Mater. Chem. 19 (2009) 8782.
[21] Z. Zhang, P. Wang, J. Mater. Chem. 22 (2012) 2456.
[22] S. Bai, J. Ge, L. Wang, M. Gong, M. Deng, Q. Kong, L. Song, J. Jiang, Q. Zhang, Y. Luo, Y. Xie, Y. Xiong, Adv. Mater. 26 (2014) 1.
[23] M.A. Mahmoud, W. Qian, M.A. El-Sayed, Nano Lett. 11 (2011) 3285.
[24] Y. Pan, S. Deng, L. Polavarapu, N. Gao, P. Yuan, C.H. Sow, Q. Xu, Langmuir 28 (2012) 12304.
[25] Y.L. Liu, Y.C. Liu, R. Mu, H. Yang, C.L. Shao, J.Y. Zhang, Y.M. Lu, D.Z. Shen, X.W. Fan, Semicond. Sci. Technol. 20 (2005) 44.
[26] E. Ko, J. Choi, K. Okamoto, Y. Tak, J. Lee, ChemPhysChem 7 (2006) 1505.
[27] D.F. Zhang, H. Zhang, L. Guo, K. Zheng, X.D. Han, Z. Zhang, J. Mater. Chem. 19 (2009) 5220.
[28] M. Chitambar, Z. Wang, Y. Liu, A. Rockett, S. Maldonado, J. Am. Chem. Soc. 134 (2012) 10670.
[29] H.I. Karunadasa, C.J. Chang, J.R. Long, Nature 464 (2010) 1329.